

# Cyclic Mathematical Morphology in Polar-Logarithmic Representation

Miguel Angel Luengo-Oroz and Jesús Angulo

**Abstract**—We propose in this paper to perform mathematical morphology operators in a geometric transformation of an image. As a result of this procedure, processing images with regular structuring elements in the transformed domain is equivalent to working with deformed structuring elements in the original representation. More specifically, the conversion into polar-logarithmic coordinates provides satisfying results in image analysis applied to round objects, if they are roughly origin-centered. We have illustrated the interest of the derived cyclic morphology with two pattern recognition examples: erythrocyte shape analysis and multiscale description of iris textures.

**Index Terms**—Circular opening, granulometric iris code, polar-logarithmic coordinates, radial skeleton, red blood cell shape analysis, spatially variant mathematical morphology.

## I. INTRODUCTION

TRANSLATION, rotation, and scale invariant representations are very useful in shape analysis applications. Usually, these representations convert visual shape information into an abstract representation such as Fourier descriptors [1]. However, these spaces may not be suitable for the intuitive processing performed by mathematical morphological operators. One of the fundamental advantages of mathematical morphology [2] applied to image processing is that it is intuitive since it works directly on the spatial domain: the shape and the size of structuring elements considered as the *basic bricks*, play the same role as frequencies do in the analysis of sound. We try to maintain this intuitive advantage for morphological image analysis and find a representation system which presents more advantages than the traditional Cartesian representation when processing images which contain some kind of radial symmetry, or in general, which have a center. The selected transformation is the polar-logarithmic representation [3]. Morphological operators through this spatially variant support space have been previously studied from a theoretical point of view in [4], [5]. However, the direct implementation of polar operators proposed in these previous works implies very high computational cost. We propose here an alternative framework which consist in firstly doing the polar-logarithmic transformation of the image; secondly performing classic morphological

operators in the transformed image and finally performing the inverse geometric transformation in order to restore the initial image modified by the operations with deformed structuring elements. We should point out the benefits of developments introduced in this paper are limited to transformations in which the object of interest remains (nearly) origin-centered.

A preliminary version of this work was presented in [6]. This paper is organized as follows. In Section II, we review the polar-logarithmic transform. In Section III, the theoretical support for cyclic morphology in the log-pol space is presented. Next, in Section IV, some morphological tools are proposed and their use is illustrated by two pattern recognition applications developed with the proposed methodology. Discussion concludes the paper.

## II. POLAR-LOGARITHMIC REPRESENTATION

### A. Geometric Transformations of Images

A geometric transformation of a digital image is an operation that converts the original image  $f(\eta)$  into the transformed image  $f(\hat{\eta})$  by applying a function  $\xi : f(\eta) \rightarrow f(\hat{\eta})$  that maps each point in the source image to its corresponding point in the destination image. A simple solution to this problem is to perform an inverse-transformation  $\xi^{-1}$  from each pixel coordinate  $\hat{\eta}$  in the destination image to a corresponding pixel location  $\eta$  in the source image. The calculated coordinates for the location of the pixel in the source image will only rarely be integers, so the calculated pixel location often lies in an area between multiple pixels in the original image. In order to solve this problem, we need to fit the discrete data to a continuous function and to calculate the corresponding interpolated value. Concerning this resampling step, the choice of the appropriate technique depends on the tradeoff between the demanded accuracy of the interpolation and the computational cost. The nearest-neighbor, bilinear, or bicubic interpolation provide enough quality in most cases; however, some applications may require more precise methods, such as spline-based models [7].

### B. Polar-Logarithmic Coordinates

The polar-logarithmic representation, or log-pol coordinates, has already been used to map the visual cortex of primates [8]: the photoreceptors of the retina are placed according to the same organization. This model of log-pol fovea is applied mainly in artificial vision systems, for instance in robotics [9]. In addition, due to its scientific utility in describing fundamental aspects of human vision, the artificial fovea has also been applied in order to assess the optical flow [10] or to recognize and track objects [11]. The polar-logarithmic transformation converts the original image  $\eta = (x, y)$  into another  $\hat{\eta} = (\rho, \omega)$  in which the angular

Manuscript received June 19, 2007; revised December 02, 2008. First published March 24, 2009; current version published April 10, 2009. This work was supported in part by the Spanish grant FPI-CM(0362/2005). The associate editor coordinating the review of this manuscript and approving it for publication was Dr. Dimitri Van De Ville.

M. A. Luengo-Oroz is with the Biomedical Image Technologies Lab of ETSI Telecomunicación, Universidad Politécnica de Madrid, 28040, Madrid, Spain (e-mail: maluengo@die.upm.es).

J. Angulo is with the Center of Mathematical Morphology of Ecole des Mines de Paris, 77305 Fontainebleau, France (e-mail: angulo@cmm.ensmp.fr).

Digital Object Identifier 10.1109/TIP.2009.2013078



Fig. 1. (a)  $\rightarrow$  (b): Example of log-pol conversion  $f(\eta) \rightarrow f(\hat{\eta})$ , where  $\eta_c$  corresponds to the center of the image, near Lena's left eye.

coordinate is placed on the vertical axis and the logarithmic coordinate is placed on the horizontal one (see Fig. 1, notice that  $(x, y)$  and  $(\rho, \omega)$  axis are placed as in Fig. 1 for all figures in the following sections). More precisely, with respect to a central point  $\eta_c = (x_c, y_c)$ :  $\rho = \log(\sqrt{(x - x_c)^2 + (y - y_c)^2})$ ,  $0 \leq \rho \leq \rho_{\max}$ ;  $\omega = \arctan((y - y_c)/(x - x_c))$ ,  $0 \leq \omega < 2\pi$ .

#### PSEUDOCODE DIRECT TRANSFORMATION

Input: Cartesian  $(x, y) \in N \times N$

$\rightarrow$  Output: Log-polar  $(r, \omega) \in M \times K$

$$\hat{x} = \frac{N/2-1}{M-1}(M-1) \frac{r}{M-1} \cos\left(\frac{2\pi\omega}{K}\right) + \frac{N}{2}$$

$$\hat{y} = \frac{N/2-1}{M-1}(M-1) \frac{r}{M-1} \sin\left(\frac{2\pi\omega}{K}\right) + \frac{N}{2}$$

#### PSEUDOCODE INVERSE TRANSFORMATION

Input: Log-polar  $(r, \omega) \in N \times N$

$\rightarrow$  Output: Cartesian  $(x, y) \in X \times Y$

$$\hat{x} = N \frac{\log\left(\sqrt{\frac{(y-Y/2)^2}{Y^2/4} + \frac{(x-X/2)^2}{X^2/4}}\right)}{\log(\sqrt{2})}$$

$$\hat{\omega} = \frac{N}{2} + \frac{N \arctan\left(\frac{y-Y/2}{Y/2}, \frac{x-X/2}{X/2}\right)}{2\pi}$$

Most of examples shown in this paper are images of size  $256 \times 256$  pixels in  $(x, y)$  coordinates and a bilinear interpolation schema has been used for the image transformation. For the sake of coherence in the figures, the  $(\rho, \omega)$  coordinates have been discretized in the same number of pixels than the Cartesian ones. However, as said above, the resolution can be increased by different interpolation schemes.

The log-pol representation presents some interesting properties. Rotations in the original Cartesian image become vertical cyclic shifts in the transformed log-pol image because of the periodic nature of the angular component. Analogously, the changes of size in the original image become horizontal shifts in the transformed image, according to the autosimilarity property of the exponential function. The choice of the center is crucial and all further treatments are sensitive to its choice (see Fig. 2). Ideally the center point should be previously defined by the nature of the object. If the center is not prefixed by any special

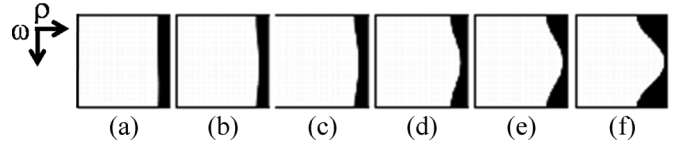


Fig. 2. Log-pol transformation centered in  $\eta_c$  of a circle whose central point is  $\eta_{\text{circle}}$  and radius  $r$ . The value of  $\eta_c$  is displaced from  $\eta_{\text{circle}}$  at different percentages of  $r$ : (a) 0%, (b) 8%, (c) 16%, (d) 32%, (e) 48%, and (f) 70%.

feature, we may chose the center of gravity or the maximum of a certain distance function, for instance the geodesic center [12].

### III. CYCLIC MORPHOLOGY

#### A. Definition

Let  $f(x, y)$  be a 2-D image defined on the discrete space  $E \subset Z^2$ ,  $\eta = (x, y) \in (Z \times Z)$ , with values of the complete lattice  $\mathcal{T}$  (for simplicity the complete lattice is considered to be  $\mathcal{T} = Z$  or a subset from  $Z$  corresponding to the grey levels  $\mathcal{T} = \{0, 1, \dots, 255\}$ ). The extension of the operators from classical mathematical morphology to the log-pol representation is achieved by changing the support of the image in order to introduce the principle of periodicity. The log-pol transformation of the function  $f(x, y)$  generates a new function image  $\hat{f}(\rho, \omega) : E_{\rho, \omega} \rightarrow \mathcal{T}$ , where the support of the image is the space  $E_{\rho, \omega}$ ,  $\hat{\eta} = (\rho, \omega) \in (Z \times Z_p)$  and where the angular variable  $\omega \in Z_p$  is periodic with period  $p$  equivalent to  $2\pi$ . A new relation of neighborhood is established between points at the top of the image ( $\omega = 0$ ) and the ones at the bottom of the image ( $\omega = p - 1$ ). Therefore, the image can be seen as a strip where the superior and the inferior borders are joined (see Fig. 3). The aim of this change is to preserve the invariance with respect to rotations in the Cartesian space, when morphological operations are done in the log-pol space.

Let  $B_{S\omega, S\rho}(\hat{\eta}) = S\omega V(\hat{\eta}) \oplus S\rho H(\hat{\eta})$  be a rectangular structuring element (SE) centered at point  $\hat{\eta}$ , where  $V(\hat{\eta})$  is the unit vertical SE and  $H(\hat{\eta})$  the unit horizontal SE, and  $S\omega$  and  $S\rho$  their respective sizes (the symbol  $\oplus$  is the Minkowski addition [2]). It is worth nothing the fact that horizontal and vertical neighborhoods respectively acquire radial and angular sense when processing in the original image representation. For instance, a vertical structuring element corresponds to an arc in the original image and a square corresponds to a circular sector. More precisely, working in the log-pol space with the SE  $B_{S\omega, S\rho}(\hat{\eta})$  is completely equivalent to work in the cartesian space with the SE  $\hat{B}_{S\omega, S\rho}(\eta, \eta_c)$  (see Fig. 3).

#### B. Implementation

The direct implementation of  $\omega$ -periodicity needs the connectivity relationship to be modified by replacing the  $y$  coordinate by  $y \bmod(y_{\max})$ . As an alternative, we propose to extend the image along its angular direction by adding the top part of the image onto the bottom and the bottom part onto the top. The size of this duplicated part on each side should be bigger than the size of the vertical component of the structuring element in order to avoid a possible

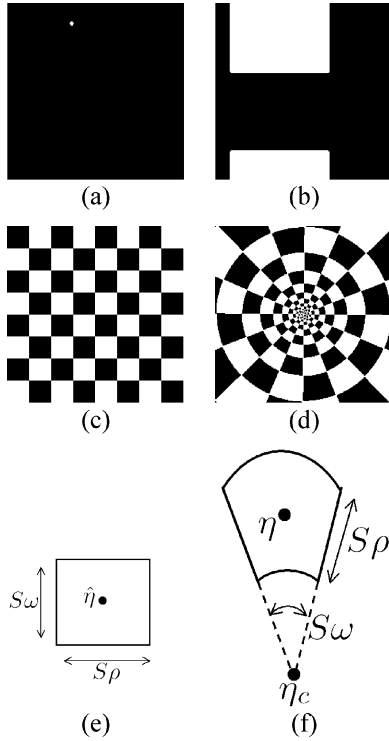


Fig. 3. (a)  $\rightarrow$  (b): Dilation of one point by a square in log-pol coordinates. (c) $\leftrightarrow$  (d): Square structuring elements in log-pol space and their equivalence in cartesian space. (e)  $\leftrightarrow$  (f):  $B_{S_w, S_\rho}(\hat{\eta})$  and its equivalence in cartesian space  $\hat{B}_{S_w, S_\rho}(\eta, \eta_c)$ .

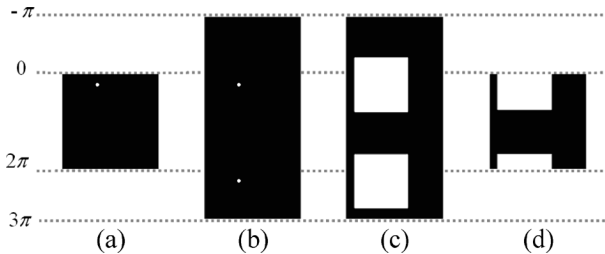


Fig. 4. Example of 2-D cyclic dilation (from left to right): (a) Original  $\rightarrow$ ; (b) cyclic image  $\rightarrow$ ; (c) dilation by a square  $\rightarrow$ ; (d) original image mask: cyclic dilation.

edge effect. After having rendered the image cyclic, morphological operators should be applied as usual and only the image corresponding to the initial mask should be kept (see Fig. 4). After this preparation of the image, all the existing code of standard implementation of morphological operators in square neighborhoods may be used unchanged.

#### IV. APPLICATIONS

In this section, we present two applications of cyclic mathematical morphology: one for shape analysis (binary images) and the other for texture description (grey-level images). Before describing these applications, we introduce the morphological operators which will be used in the sequel.

##### A. Morphological Tools

- *Circular filtering by openings/closings.*

The basic morphological operators are the *erosion*, i.e.,  $\varepsilon_{B_{S_w, S_\rho}}(\hat{f})(\hat{\eta})$  and the *dilation*, i.e.,  $\delta_{B_{S_w, S_\rho}}(\hat{f})(\hat{\eta})$ . The two elementary operations of erosion and dilation can be composed together to yield a new set of operators having desirable filtering properties which are given by the *opening*, i.e.,  $\gamma_{B_{S_w, S_\rho}}(\hat{f})(\hat{\eta}) = \delta_{B_{S_w, S_\rho}}[\varepsilon_{B_{S_w, S_\rho}}(\hat{f})](\hat{\eta})$ , and the *closing*, i.e.,  $\varphi_{B_{S_w, S_\rho}}(\hat{f})(\hat{\eta}) = \varepsilon_{B_{S_w, S_\rho}}[\delta_{B_{S_w, S_\rho}}(\hat{f})](\hat{\eta})$ . The morphological *openings* (*closings*) filter out positive (negative) peaks from the structures according to the predefined size and shape of structuring element  $B_{S_w, S_\rho}(\hat{\eta})$ . Extracting inclusions or extrusions from the contour of a relatively rounded binary shape with simple log-pol openings  $\gamma_{B_{S_w, S_\rho}}$  or closings  $\varphi_{B_{S_w, S_\rho}}$  is the most direct application of cyclic morphology [see Fig. 5(a)].

A morphological tool that complements opening/closing operators for extraction of marked particles is the morphological reconstruction, implemented using the *geodesic dilation*, operator based on restricting the iterative dilation of a function marker  $\hat{f}_m(\hat{\eta})$  by the unitary structuring element  $B_{1,1}$  to a function reference  $\hat{f}_r(\hat{\eta})$ , i.e.,  $\delta_{\hat{f}_r}^{(n)}(\hat{f}_m) = \delta_{\hat{f}_r}^{(1)}\delta_{\hat{f}_r}^{(n-1)}(\hat{f}_m)$ , where  $\delta_{\hat{f}_r}^{(1)}(\hat{f}_m) = \delta_{B_{1,1}}(\hat{f}_m(\hat{\eta})) \wedge \hat{f}_r(\hat{\eta})$ . The reconstruction by dilation or *opening by reconstruction* is then defined as  $\gamma^{\text{rec}}(\hat{f}_m, \hat{f}_r) = \delta_{\hat{f}_r}^{(i)}(\hat{f}_m)$  such that  $\delta_{\hat{f}_r}^{(i)}(\hat{f}_m) = \delta_{\hat{f}_r}^{(i+1)}(\hat{f}_m)$  (idempotence). The definition of *closing by reconstruction*  $\varphi^{\text{rec}}(\hat{f}_m, \hat{f}_r)$  is obtained by duality. Whereas the adjunction opening  $\gamma_{B_{S_w, S_\rho}}(\hat{f})$  (from an erosion/dilation) modifies the structures of the image, the associated opening by reconstruction  $\gamma^{\text{rec}}(\hat{f}_m, \hat{f})$  (where the marker  $\hat{f}_m = \varepsilon_{B_{S_w, S_\rho}}(\hat{f})$  or  $\hat{f}_m = \gamma_{B_{S_w, S_\rho}}(\hat{f})$ ) is aimed at efficiently and precisely reconstructing the “shape” of the structural peaks which are not totally removed by the marker filtering process (peaks of size  $B_{S_w, S_\rho}$ ).

- *Radial skeletons.*

The concept of skeleton of a binary set  $X$  is very intuitive, however, its mathematical definition is not simple [13]. We propose to build the morphological skeletons using the thinning transformation. The *skeleton by thinning*,  $\text{Thin}(X)$ , is the application until stability of the hit-or-miss operator according to a predefined family of patterns. See in [2] details on the suitable series of patterns to be used to obtain homotopic skeletons. Using cyclic morphology, we define a *radial inner skeleton*  $sk^{\text{in}}(f(\eta)) = \text{Thin}(\hat{f}(\hat{\eta}))$  as the skeleton obtained by homotopic thinning from the log-pol transformation of an objet  $f(\eta)$ . The invert transformation to Cartesian coordinates from the branches of the radial inner skeleton has radial sense and tends to converge on the center ( $\rho = 0$ ). We also define the *radial outer skeleton* as the skeleton obtained by an homotopic thickening of the image,  $\hat{f}^c(\hat{\eta})$  of the log-pol transformation of the object,  $sk^{\text{out}}(f(\eta)) = \text{Thin}(\hat{f}^c(\hat{\eta}))$ . The inverse transformation to Cartesian coordinates from the branches of the radial outer skeleton has also radial sense and this time, they tend

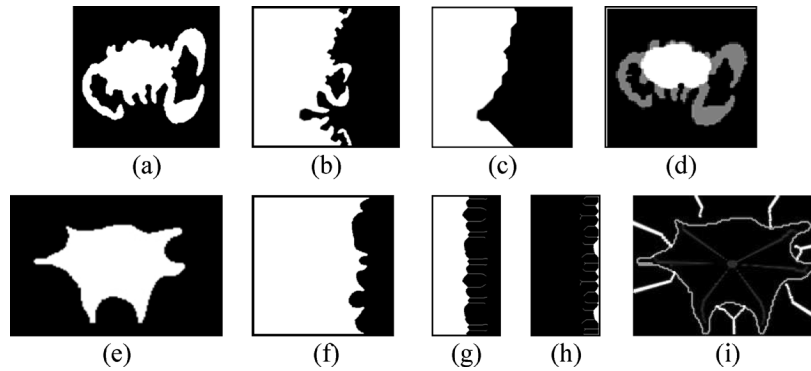


Fig. 5. Top row, extremities segmentation from “Leirus quinquestratus”: (a) Original Cartesian image; (b) log-pol image (the center is the central image point); (c) opening in log-pol space with a vertical structuring element  $S\omega = \pi/5$ ; (d) effect of filtering in Cartesian image. Bottom row, radial from an “Achantocyte” (red blood cell): (e) original Cartesian image; (f) log-pol image (the center is the central image point); (g)–(h) radial inner and radial outer skeletons respectively on cycled version of log-pol image; (i) effect of radial skeletons in Cartesian image.

to diverge to an hypothetical circumference in the infinity ( $\rho \rightarrow \infty$ ) [see Fig. 5(b)].

- *Cyclic rectangular granulometry.*

A granulometry is the study of the size/shape structure distribution of an image. We focus here on rectangular granulometries, which uses rectangular SE and have been previously used to characterize document images [14]. Using horizontal/vertical operators in the log-pol representation, this shape and texture descriptor is specially adapted to analyze images with multiscale radial and angular patterns. Formally, a *granulometry* can be defined as an indexed family of transformations  $\Gamma = (\gamma_{B_{S\omega, S\rho}})_{S\omega \geq 0, S\rho \geq 0}$ , such that  $\gamma_{B_{S\omega, S\rho}}$ , or more generally  $\Gamma$ , verifies:

- 1)  $\gamma_0$  is the identity mapping; i.e.,  $\gamma_0(f) = f$ ;
- 2)  $\gamma_\lambda$  is increasing; i.e.,  $f \leq g \Rightarrow \gamma_\lambda(f) \leq \gamma_\lambda(g), \forall \lambda \geq 0$ , for every  $f$  and  $g$ ;
- 3)  $\gamma_\lambda$  is anti-extensive; i.e.,  $\gamma_\lambda(f) \leq f, \forall \lambda \geq 0$ , for every  $f$ ;
- 4)  $\gamma_\lambda$  follows the absorption law; i.e.,  $\forall \lambda \geq 0, \forall \mu \geq 0$ ,  $\gamma_\lambda \gamma_\mu = \gamma_\mu \gamma_\lambda = \gamma_{\max(\lambda, \mu)}$ .

In particular, these axioms are valid for the adjunction opening  $\gamma_{B_{S\omega, S\rho}}(f) = \delta_{B_{S\omega, S\rho}} \varepsilon_{B_{S\omega, S\rho}}(f)$  or for the opening by reconstruction  $\gamma_{B_{S\omega, S\rho}}(f, f)$ . Granulometries by *closings* (or *anti-granulometry*) can also be defined as families of increasing closings  $\Phi = (\varphi_{B_{S\omega, S\rho}})_{S\omega \geq 0, S\rho \geq 0}$ . Performing the granulometric analysis of an image in log-pol  $\hat{f}(\hat{\eta})$  with  $\Gamma$  is equivalent to measuring the area of the opened image  $\mathcal{M}(\gamma_{B_{S\omega, S\rho}}(\hat{f}))$  after each opening of sizes  $S\omega$  (angular)  $S\rho$  (radial), where  $\mathcal{M}(\hat{f}(\hat{\eta}))$  is the Lebesgue measure of the image  $\hat{f}(\hat{\eta})$  ( $\mathcal{M}$  is the *area* in the binary case and the *volume* in the grey scale case). The *cyclic size distribution* of  $\hat{f}(\hat{\eta})$  with respect to  $\Gamma$ , denoted  $CSD_f^\Gamma(S\omega, S\rho)$  is defined as the following (normalized) mapping  $CSD_f^\Gamma(S\omega, S\rho) = (\mathcal{M}(\hat{f}) - \mathcal{M}(\gamma_{B_{S\omega, S\rho}}(\hat{f}))) / \mathcal{M}(\hat{f})$ . The size distribution  $CSD_f^\Gamma(S\omega, S\rho)$  maps each angular/radial size  $(S\omega, S\rho)$  to some measure of the positive structures with this size. The size distribution of dark structures is obtained from a family of closings, i.e.,  $CSD_f^\Phi(S\omega, S\rho) = (\mathcal{M}(\varphi_{B_{S\omega, S\rho}}(\hat{f})) - \mathcal{M}(\hat{f})) / \mathcal{M}(\hat{f})$ .

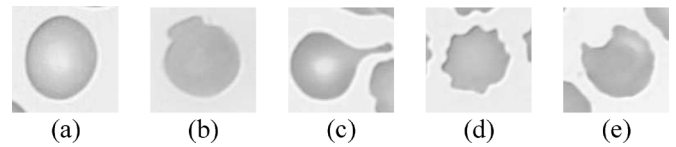


Fig. 6. Different typologies of red blood cells: (a) Normal erythrocyte; (b) “Mushroom” erythrocyte; (c) “Spicule” erythrocyte; (d) “Echinocyte” erythrocyte; (e) “Bitten” erythrocyte.

Another useful measure is the pattern spectrum [15], calculated as the derivative of size distribution  $CSD_f^\Gamma$  with respect to  $S\omega$  or  $S\rho$ .

### B. Application to the Erythrocyte Shape Analysis

In hematology, the visual analysis of the morphology of erythrocytes (size, shape, color, center, . . .) is of vital importance as it is well known that anomalies and variations from the typical red blood cell are associated with anemia or other illnesses [16]. In Fig. 6, a selection of abnormal erythrocytes is shown. We present hereafter one of the algorithms dedicated to the shape analysis developed in the MATCHCELL2 project [17], [18].

The aim of the proposed algorithm is to extract the inclusions from the erythrocyte shape, which is ideally round. This algorithm is used to identify the “bitten” class. It starts with the binary mask of the segmented erythrocyte, image (A), and its centroid  $\eta_c$ . The results correspond to image (E) (see Fig. 7); if  $(E) \neq \emptyset$  and the verifications are confirmed, it is classified as “bitten” erythrocyte (we have considered the gravity center as the center of the log-pol transformation).

- 1) Log-pol transformation  $(A) \Rightarrow (B) = \xi_{\eta_c}(A)$ .
- 2) Radial outer skeleton  $(B) \Rightarrow (C) = sk^{\text{out}}(B)$ .
- 3) Circular filtering: Residue from a vertical closing of size  $S\omega = \pi/3$  (maximal admissible angle for the inclusion)  $(B) \Rightarrow (D) = \varphi_{\pi/3}(B) - (B)$  are the inclusion candidates.
- 4) Geodesic reconstruction of (D) using the marker (C)  $\Rightarrow (E) = \gamma^{\text{rec}}((C), (D))$ .
- 5) We verify that  $\forall E_i$  connected subset  $\in (E)$ ,  $[\text{Surface}(E_i) / \text{Sizeimage}] > \mu_1$ .

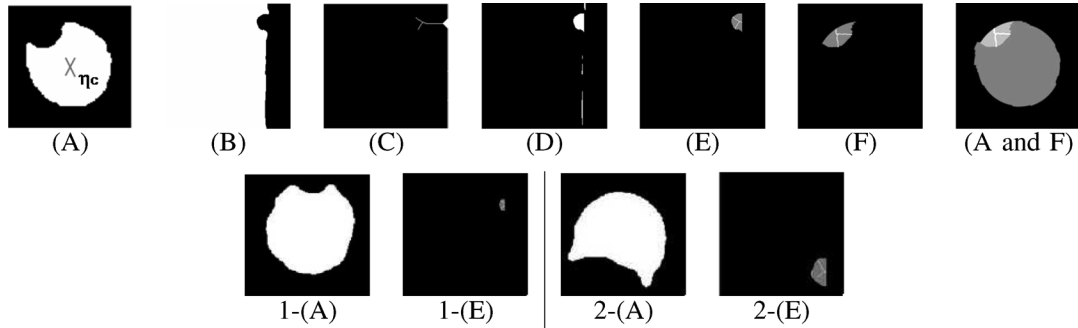


Fig. 7. Top row, extrusion extraction algorithm for “bitten” erythrocytes. Bottom row, other examples of “bitten” extraction (1,2).

#### 6) Inverse transformation $(E) \Rightarrow (F) = \xi^{-1}(E)$ .

The algorithm has an efficient and robust performance in the extraction of inclusions and extrusions. The use of the skeleton in order to sieve the candidates gives much greater robustness than would a mere opening or closing. This procedure removes small connected components preselected as deformations. Furthermore, the examples corresponding to “echinocytes,” “spicules,” and “mushroom” have been correctly classified (see more examples and details in [17]).

### C. Application to Biometric Iris Identification

Iris texture patterns are considered to be different for each person and to remain stable over time. This interclass variability makes iris recognition one of the most interesting techniques for security applications, as very high recognition rates have been reported for iris identification systems [19]. However, only a few large-scale experiment evaluations have been reported, and there are insufficient publicly available databases. Further work in this field remains to be done, especially in validation and concerning with non ideal quality images. An iris recognition system can be divided into four parts: data acquisition, iris segmentation, iris feature extraction and classification. In this work, we just deal with the iris feature extraction. The goal is to produce a compact codification of the iris patterns from the segmented iris image which is made by a multiscale decomposition. The best known and proved system has been proposed by Daugman [20] and the encoding of the iris is done through the application of 2-D Gabor wavelet. Other methods use a Laplacian pyramid decomposition [21] or zero-crossing wavelet transform [22]. Regarding morphological approaches, a work based on skeletons representations of the iris patterns has been also proposed [23]. However, this method suffers from lack of robustness.

We propose to characterize the iris pattern by a grey-scale cyclic rectangular granulometry of openings by reconstruction and closings by reconstruction. Therefore, after eye’s segmentation, each eye pattern in log-pol coordinates  $\hat{f}_{seg}$  is characterized by the two bivariate histograms  $CSD_{\hat{f}_{seg}}^{\Gamma_{rec}}(S\omega, S\rho)$  and  $CSD_{\hat{f}_{seg}}^{\Phi_{rec}}(S\omega, S\rho)$  (see Fig. 8). Note that the use of openings and closings by reconstruction for the multiscale representation preserves contour information of the decomposed iris patterns (see Fig. 9). The measurements  $CSD_{\hat{f}}^{\Gamma_{rec}}(S\omega, S\rho)$  and

$CSD_{\hat{f}}^{\Phi_{rec}}(S\omega, S\rho)$  permit to describe the morphological size distribution of the different structures under a radial-angular metric. Tested images have shown interesting discriminative properties for the selected descriptors. This representation is invariant under size changes and rotations (which may be a problem due to the non perfect alignment of the user’s head). Concerning the computational complexity, it is possible to perform a very efficient implementation by decomposing the rectangular SE in linear SE [24]. In relation to the next step in the biometric identification procedure, a codification of the CSD surfaces should be extracted to obtain the user’s key. As it is desired to have a small key, the length  $S\rho$  and  $S\omega$  of the unit linear SE should be correlated to the quantity of information chosen for the codification (notice that the variation of the unit linear SE length provides a subsampling of the CSD surfaces).

The proposed methodology is currently being validated in larger databases. In first experiments, multivariate cyclic granulometries and its derived measurements show promising results as an alternative to wavelet analysis in iris biometric characterization.

## V. DISCUSSION

We have presented the general framework for cyclic morphology and some basic morphological tools adapted to this representation. Two pattern recognition examples developed with these operators have been presented.

The fundamental idea is that processing images in an intuitive geometric space can provide advantages over the traditional Cartesian representation. Regarding specifically mathematical morphology, the key issue is to obtain structuring elements that are adapted to the nature of the objects to be analyzed, not by deforming them (such as in morphological amoebas [25] or in viscous operators [26]), but by transforming the image itself. We consider that applying morphological operators with regular structuring elements in the transformed domain is equivalent to work with deformed structuring elements in the original image. Not only adapted metrics may be used, but also this kind of process provides benefits in terms of computational costs. More specifically, the conversion into polar-logarithmic coordinates as well as the derived cyclic morphology provides satisfying results in image analysis applied to round objects or spheroid-shaped 3-D-object models. The study of more complex morphological operators in the log-pol space still remains

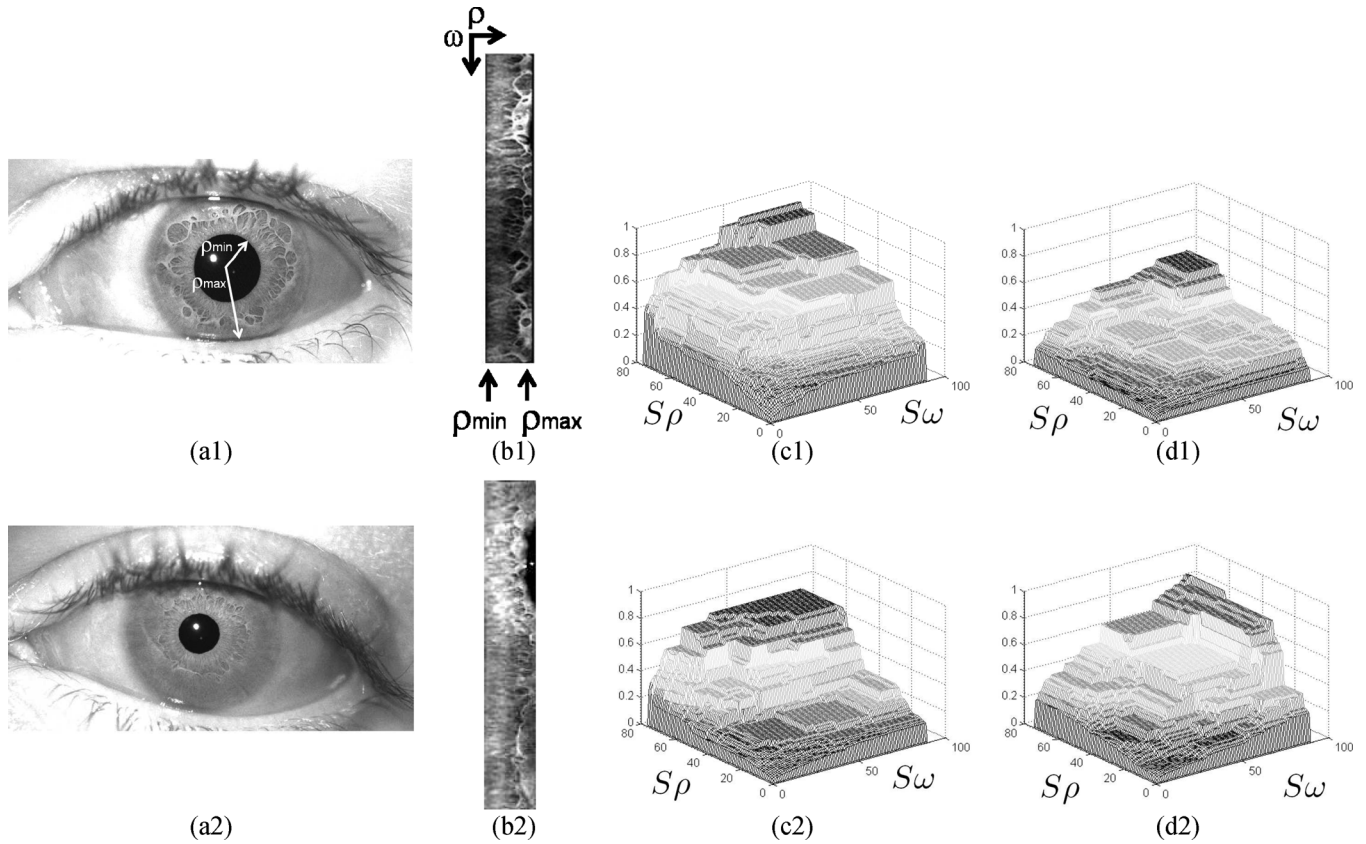


Fig. 8. Morphological description of two iris patterns: (a) Eye image ( $f$ ); (b) segmented iris pattern in log-pol coordinates ( $\hat{f}_{\text{seg}}$ ); (c)  $CSD_{\hat{f}_{\text{seg}}}^{\text{rec}}(S\omega, S\rho)$ ; (d)  $CSD_{\hat{f}_{\text{seg}}}^{\text{rec}}(S\omega, S\rho)$ .

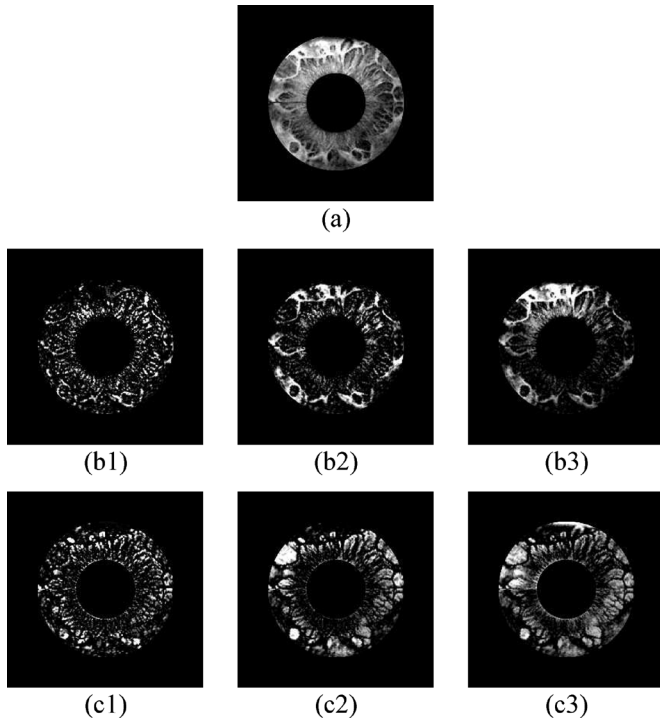


Fig. 9. Iris morphological decomposition: (a) Segmented iris pattern ( $f_{\text{seg}}$ ); (b) cyclic opening-by-reconstruction top-hat ( $f_{\text{seg}} - \gamma_{B_{S\omega, S\rho}}^{\text{rec}}(f_{\text{seg}})$ ); (c) cyclic closing-by-reconstruction bottom-hat ( $\varphi_{B_{S\omega, S\rho}}^{\text{rec}}(f_{\text{seg}}) - f_{\text{seg}}$ ). The SE size ( $S\omega, S\rho$ ) used in the examples are:  $b1(1/\pi, 20\%)$ ,  $b2(\pi/6, 1\%)$ ,  $b3(\pi/6, 20\%)$ ,  $c1(1/\pi, 20\%)$ ,  $c2(\pi/6, 1\%)$ ,  $c3(\pi/6, 20\%)$ .

an open topic, as well as the possibility to work under other geometric transformations.

ACKNOWLEDGMENT

The authors would like to thank F. Meyer, M. Huertas, G. Flandrin, J. Klossa, and C. Sanchez-Avila for fruitful discussions and their collaboration in the experimental sections.

REFERENCES

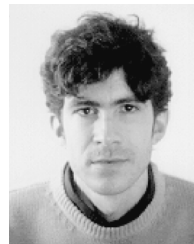
- [1] C. Zahn and R. Roskies, "Fourier descriptors for plane closed curves," *IEEE Trans. Comput.*, vol. 21, pp. 269–281, Mar. 1972.
- [2] J. Serra, *Image Analysis and Mathematical Morphology*. London, U.K.: Academic, 1982, 1988, vol. I,II.
- [3] C. Weiman and G. Chaikin, "Logarithmic spiral grids for image processing and display," *Comput. Graph. Image Process.*, vol. 11, pp. 197–226, 1979.
- [4] H. J. A. M. Heijmans and C. Ronse, "The algebraic basis of mathematical morphology. i dilations and erosions," *Comput. Vis., Graph., Image Process.*, vol. 50, no. 3, pp. 245–295, 1990.
- [5] J. B. T. M. Roerdink, "Group morphology," *Pattern Recognit.*, vol. 33, no. 6, pp. 877–895, 2000.
- [6] M. A. Luengo-Oroz, J. Angulo, G. Flandrin, and J. Klossa, "Mathematical morphology in polar-logarithmic coordinates. application to erythrocyte shape analysis," in *Proc. IbPRIA (2)*, 2005, pp. 199–206.
- [7] M. Unser, "Splines: A perfect fit for signal and image processing," *IEEE Signal Process. Mag.*, vol. 16, no. 6, pp. 22–38, Jun. 1999.
- [8] E. Schwartz, "Spatial mapping in the primate sensory projection: Analytic structure and relevance to perception," *Biol. Cybern.*, vol. 27, pp. 181–194, 1977.
- [9] M. Bolduc and M. D. Levine, "A review of biologically motivated space-variant data reduction models for robotic vision," *Comput. Vis. Image Understand.*, vol. 69, no. 2, pp. 170–184, 1998.

- [10] M. Tistarelli and G. Sandini, "On the advantages of polar and log-polar mapping for direct estimation of time-to-impact from optical flow," *IEEE Trans. Pattern Anal. Mach. Intell.*, vol. 15, no. 4, pp. 401–410, Apr. 1993.
- [11] A. Bernardino and J. Santos-Victor, "A binocular stereo algorithm for log-polar foveated systems," in *Proc. Biologically Motivated Computer Vision*, 2002, pp. 127–136.
- [12] C. Lantuejoul and F. Maisonneuve, "Geodesic methods in quantitative image analysis," *Pattern Recognit.*, vol. 17, no. 2, pp. 177–187, 1984.
- [13] C. Lantuejoul, "La squelettisation et son application aux mesures topologiques des mosaïques polycristallines," Ph.D. dissertation, School Mines of Paris, Paris, France, 1978.
- [14] A. D. Bagdanov and M. Worring, "Multi-scale document description using rectangular granulometries," *Document Anal. Syst.*, pp. 445–456, 2002.
- [15] P. Maragos, "Pattern spectrum and multiscale shape representation," *IEEE Trans. Pattern Anal. Mach. Intell.*, vol. 11, no. 7, pp. 701–716, Jul. 1989.
- [16] P. J. H. Bronkorsta, M. J. T. Reinders, E. A. Hendriks, J. Grimbergen, R. M. Heethaar, and G. J. Brakenhoff, "On-line detection of red blood cell shape using deformable templates," *Pattern Recognit. Lett.*, vol. 21, no. 5, pp. 413–424, 2000.
- [17] M. A. Luengo-Oroz, "Morphologie mathématique en coordonnées logarithmique-polaires et méthodes géométriques de classification. Application à l'étude des érythrocytes," M.S. thesis, School Mines Paris, Paris, France, 2004.
- [18] J. Angulo, "Morphologie mathématique et indexation d'images couleur. application à la microscopie en biomédecine," Ph.D. dissertation, School Mines Paris, Paris, France, 2003.
- [19] J. Daugman, "Probing the uniqueness and randomness of iris codes: Results from 200 billion iris pair comparisons," *Proc. IEEE*, vol. 11, pp. 1927–1935, 2006.
- [20] J. Daugman, "High confidence visual recognition of persons by a test of statistical independence," *IEEE Trans. Pattern Anal. Mach. Intell.*, vol. 15, no. 11, pp. 1148–1161, Nov. 1993.
- [21] R. P. Wildes, "Iris recognition: An emerging biometric technology," *Proc. IEEE*, vol. 85, pp. 1348–1363, 1997.
- [22] C. Sanchez-Avila and R. Sánchez-Reillo, "Two different approaches for iris recognition using gabor filters and multiscale zero-crossing representation," *Pattern Recognit.*, vol. 38, no. 2, pp. 231–240, 2005.
- [23] J. de Mira, Jr. and J. Mayer, "Identification of individuals through the morphological processing of the iris," in *Proc. Int. Conf. Image Processing*, 2003, pp. 341–344.
- [24] L. Vincent, "Granulometries and opening trees," *Fundam. Inf.*, vol. 41, no. 1–2, pp. 57–90, 2000.
- [25] R. Lerallut, E. Decencière, and F. Meyer, "Image filtering using morphological amoebas," *Image Vis. Comput.*, vol. 25, no. 4, pp. 395–404, 2007.
- [26] C. Vachier and F. Meyer, "The viscous watershed transform," *J. Math. Imag. Vis.*, vol. 22, no. 2–3, pp. 251–267, 2005.



**Miguel Angel Luengo-Oroz** received the M.S. degree in telecommunications engineering from the Universidad Politécnica de Madrid (UPM), Spain, in 2004, with a M.S. thesis on mathematical morphology at the School of Mines, Paris, France. He received the M.S. degree in cognitive science from l'École Normale Supérieure and l'École des Hautes Etudes en Sciences Sociales, France, in 2005. He is currently pursuing the Ph.D. degree with a dissertation on biomedical engineering at the Biomedical Image Technologies Lab (UPM).

He is an associate researcher at the Complex Systems Institute, Paris. His main research interests are biomedical image processing, mathematical morphology, and biological complex systems.



**Jesús Angulo** was born in Cuenca, Spain, in 1975. He received a degree in telecommunications engineering from the Polytechnical University of Valencia, Spain, in 1999, with a M.S. thesis on image and video processing, and the Ph.D. degree in mathematical morphology and image processing from the Ecole des Mines de Paris, France, in 2003, under the guidance of Prof. J. Serra.

He is currently a permanent researcher at the Center of Mathematical Morphology, MINES ParisTech. His research interests are in the areas of multivariate image processing (color, hyper/multispectral, temporal series, tensor imaging) and mathematical morphology (filtering, segmentation, shape and texture analysis, stochastic approaches, geometry), and their applications to biomedicine and biotechnology.